3   GENERAL METHOD

3.1   SUBJECTS

Data were gathered from 10 PTSD patients and 10 normal controls who were matched for sex (7 males, 3 females), age (Control: 47.4 ± 3.3 years [range 42 - 52 years], PTSD: 50.8 ± 4.6 years [range 43 - 57 years], $t[18] = -1.88$, *ns*), education (Control: 11.6 ± 2.2 years, PTSD: 11.1 ± 1.5 years, $t[18] = 0.60$, *ns*), and estimated premorbid IQ (NART-R, Crawford, 1992; Control: 109.4 ± 5.9, PTSD: 108.6 ± 3.0, $t[18] = 0.39$, *ns*). Research funding only permitted 10 subjects per group, as this study was conducted as part of a multi-modal brain imaging project that employed positron emission tomography (PET), a more expensive technology that EEG/ERPs. No subject had any history of neurological disorder or head injury. All controls had normal scores for psychological health questionnaires and they had infrequent or no use of psychoactive substances (i.e., caffeine, alcohol, tobacco, cannabis, amphetamine & opiates). Patients were free of psychoactive medication for at least two weeks before EEG collection, as it has been shown that medications improve cognitive capacities in patients and normalize P3 amplitude in PTSD patients (see Metzger et al., 1997). No patients were treated with electro-convulsive therapy (ECT) within, at least, three months prior to the study. All subjects were right handed (Annette, 1970), with normal corrected visual acuity (Snellen's chart, see Bailey & Lovie, 1976) and normal color vision (Ishihara, 1968).

Psychiatrists with expertise in PTSD diagnosed patients (Alexander McFarlane & Phillip Morris), in accordance with the *Diagnostic and Statistical Manual of Mental Disorders* (DSM-IV; American Psychiatric Association, 1994). Patients experienced various traumas, including motor vehicle accidents (3), police and fire officer duties (3),

war service (2), a natural disaster (1), and a farm accident (1). The duration of PTSD suffered varied from 2.5 years to 26 years (9.9 ± 8.8 years). Several patients had lifetime history of comorbidity, but all patients were free of current comorbidity for depression, alcohol dependence, and other anxiety disorders. Symptom severity was measured using the Impact of Event Scale (IES; Horowitz, Wilner, Alvarez, 1979) and the clinician-administered PTSD scale (CAPS; Blake et al., 1995). Anxiety and depression were measured using the State-Trait Anxiety Inventory (STAI; Spielberger, Gorsuch, Lushene, Vagg, & Jacobs, 1983) and the Beck Depression Inventory (BDI; Beck & Steer, 1987).

The experimental protocol was approved by the Social and Behavioral Ethics Committee of Flinders University and was conducted in conformance with the "Statement on Human Experimentation and Supplementary Notes" issued by the National Health and Medical Research Council (NHMRC) Australia. Both controls and patients were provided with written information concerning the procedures. Patients were assessed as competent to give consent by their referring psychiatrist. Written consent was obtained from all subjects.

3.1.1   Clinical Symptom Status

The IES indicated that patients were suffering from substantial symptoms of intrusion (25.8 ± 9.8) and avoidance (20.5 ± 10.8; IES total: 46.3 ± 18.9). CAPS ratings also indicated significant symptoms (CAPS Total: 74.9 ± 20.7; Frequency: 38.2 ± 10.1; Intensity: 36.7 ± 11.3), including intrusion (B: 15.6 ± 8.9), avoidance (C: 31.7 ± 10.8), and hyperarousal (D: 27.6 ± 6.5). In comparison with controls, patients had higher anxiety (State Anxiety, Control: 29.4 ± 7.7, PTSD: 52.8 ± 8.6, $t[18] = -6.39$, $p<.001$; Trait Anxiety, Control: 33.3 ± 6.9, PTSD: 58.8 ± 12.9, $t[18] = -5.52$, $p<.001$) and depression (BDI; Control: 5.2 ± 4.4, PTSD: 24.8 ± 9.4, $t[18] = -5.97$, $p<.001$). PTSD

patients also had poorer ratings of general psychological health than controls (GHQ; Control: 2.2 ± 3.9, PTSD: 20.6 ± 10.1, $t[18] = -5.40$, $p<.001$).

3.2 MATERIALS AND PROCEDURE

3.2.1 Subject Inclusion/Exclusion Procedure

Subjects were to be between 20-60 years of age. Any subjects were excluded if they had any history of: head injury, accidental loss of consciousness for more than one hour, any neurological abnormality (e.g., epilepsy), any developmental disabilities, psychoactive substance abuse, or essential psychoactive medication requirements that could not be denied for at least 2 weeks.

Subjects who were not excluded on the basis of the above information were assessed for normal visual acuity (Snellen eye chart), normal color vision (Ishihara, 1968), handedness (Annett, 1970), and a very simple English language assessment. Subjects were excluded if they *did not*: (a) correctly identify level 9 of the Snellen eye chart with corrected vision from both eyes, (b) correctly read the following Ishihara color plates (answer in brackets): 1 (12), 4 (29), 8 (15), 12 (97), 16 (16), 20 (no numeral), (c) use their right hand for 10 or more activities of Annett's handedness questionnaire, and (d) complete simple English language tasks.

Subjects were also screened with a computer psychiatric screening interview (Bucholz et al., 1991) and a questionnaire booklet, which included the STAI, the BDI, and a short form of the General Health Questionnaire (GHQ; Goldberg, 1970). Control subjects were excluded if they had any history of psychiatric disorder and they did not score below the following values on these questionnaires: (a) STAI < 40, (b) BDI < 10, (c) GHQ < 5.

3.2.2   Cognitive Tasks

The study was designed to probe various aspects of executive function, using an efficient task design to provide all required component processes and comparisons. There were three aspects of executive function to be evaluated: selective attention, working memory and executive attention. The following task design provided the ability to measure all of these.

Two visual tasks consisted of an identical series of red and blue words, with two different task instructions. The first task was a *fixed target* task that required detection of a specific word in a given color. This is an example of the fixed target task instructions:

> *In the next task, please attend to BLUE words and ignore RED words. You should respond quickly and accurately to any occurrence of the word CITY presented in the BLUE color only.*

The other task was a *variable target* task that required detection of any repeated words in a given color. This is an example of the variable target task instructions:

> *In the next task, please attend to RED words and ignore BLUE words. You should respond quickly and accurately to any word presented in RED that is the same as the previous RED word.*

These instructions were presented on screen before each task block began, in black text on a white background. The example of the attended target word in the task instructions was not presented in color, so subjects did not have a sensory example of all target features. This encouraged a semantic encoding of the target attributes.

There were at least three stimulus types in each task. Firstly, there were attended and unattended commons, which were differentiated by color. In addition, there were attended targets. In the fixed target task, there was a specific target word. In the variable target task, target words were identical to a preceding word in the same color.

These stimulus types were compared to provide specific estimates of component processes (see Figure 3-1).

3.2.2.1 *Task condition comparisons*

A measure of *selective attention* was obtained from the fixed target task by comparison of attended versus unattended commons. The fixed target task does not demand any working memory updating to common stimuli (see below), so differences in attended and unattended common ERPs reveal only greater attention to words in the attended color. It is argued that this allocation of attention comprises two elements: stimulus selection and stimulus comparison. Attended stimuli are first selected on the basis of color and then compared with a working memory representation of target attributes. For common stimuli, this latter comparison fails to match, so no further stimulus or response processing is required.

A measure of *working memory updating* was obtained by comparison of attended commons in the variable versus fixed target task. The fixed target task does not demand any working memory updating for common stimuli. However, the variable target task requires that the attributes of the attended common stimulus are remembered so that they can be compared with those of the next attended stimulus. Should the next attended stimulus be different from the previous one, it must displace the current working memory stimulus so that it can be remembered and compared with an ensuing attended stimulus. This *working memory updating* can be evaluated in this comparison. This comparison eliminates all sensory and perceptual stimulus processing related to the common stimuli, as these processes are common in both tasks.

A conventional measure of *executive attention or target detection* was obtained from the fixed target task by comparison of attended targets versus commons. This task is similar, in some respects, to a conventional oddball task design, with common stimuli

and occasional targets. The common stimuli require sensory/perceptual processing and a short comparison with the target attributes. On the other hand, targets require all of these processes plus the additional processes of target detection and response initiation and execution. This comparison reveals these extra processes.

Task Targets:	Fixed	Fixed	Variable	Fixed
Stimulus:	Unattend Common	Attend Common	Attend Common	Attend Target
Perception	■	■	■	■
Feature Selection	▨	▮	■	■
Evaluation	▨	▮	■	■
Working Memory Updating	▨	▨	▤	▨
Target Recognition	▨	▨	▨	▦
Motor Response	▨	▨	▨	▦

Figure 3-1. Simple schematic diagram of cognitive task comparisons: (a) the *selective attention* comparison is given in red vertical bars, where the attended common is compared with the unattended common in the fixed target task, (b) the *working memory* comparison is given in green horizontal bars, where the attended common words are compared for the variable and the fixed target tasks, and (c) the *target detection* comparison is given in a blue grid, where the attended target is compared with the attended common of the fixed target task. The black squares indicate engaged processes while the grey squares indicate absence of these processes for a stimulus condition. The component processes are discussed in detail in the following results chapters (see also Rösler et al., 1986).

3.2.2.2 Task block design

Each task block comprised a pseudo-random series of red and blue, lower case, concrete nouns of between four and seven letters, with no more than two syllables. The words were presented at a fixed intensity to the centre of a black screen in Arial 48 points for 200 ms, with a random stimulus onset asynchrony of 1.6-1.7 sec. Words

were presented in blocks of 60, consisting of ten different words, such that five words appeared five times in red and once in blue and the other five words appeared five times in blue and once in red. The constraints on the randomized presentation were that all consecutive repeats in one color were separated by only one word in the other color and there were no consecutive repeats of 3 or more words. The sequence of words was very carefully designed to provide the ability to extract various stimulus conditions for the fixed and the variable target task instructions.

For each block of 60 words in the fixed target task, there were four stimulus types: attended targets (5/60, 8.3%), attended commons (25/60, 41.6%), unattended commons (29/60, 48.3%), and an unattended target (1/60, 1.6%).

In the variable target task, which used the same stimulus sequence as the fixed target task, there were six stimulus types. The proportion of attended targets was 5/60 (8.3%), attended commons was 20/60 (33.3%), and unattended commons was 20/60 (33.3%). There were several consecutive repeats in the unattended color (termed unattended targets 5/60, 8.3%), which constitute the attended targets when the same stimulus sequence is used with the opposite color attended. Also, there were a few repeats of the same word in opposite colors, which were designated unattended distracters if the unattended color followed the attended color (5/60, 8.3%) or attended distracters if the attended color followed the unattended color (5/60, 8.3%; the task design was planned to provide useful data for these distracters, but the signal-to-noise ratio precluded effective analyses). Note that target words were separated by one unattended common, so the target detection process could not rely on visual memory alone, although it was a relatively short retention period. For the non-target words, retention periods were longer intervals, as the attended common words were separated by at least 3 unattended words, which entail a retention interval of 1.6-6.8 sec. The unattended common words in this task were not used to assess selective attention for

color, as they could evoke not only stimulus feature discrimination, but also a greater degree of controlled inhibition than the unattended commons for the fixed target task (unfortunately time did not permit careful evaluation of this hypothesis).

3.2.2.3   Task Procedure

To ensure the words presented were not associated with patient trauma, each subject rated words on a scale from 1 to 10, where 1 indicates neutrality and 10 indicates trauma association. Words presented rated at less than four. Hence, the words presented were different for each subject, although all words were selected from a large set of 300 words that conform to the requirements above. It was not possible to identify the mean frequency of use in English for all of the words, although a conscientious effort was made to use medium frequency words.

Tasks were performed in a special air-conditioned room, fitted with a Faraday cage. The stimulus sequences and response measurement were coordinated with NeuroScan *STIM* software, using a Viewsonic 15" color monitor, placed 60 cm from the eyes. Response speed and accuracy were equally emphasized in task instructions and subjects responded by pressing a *STIMPAD* button with their right index finger.

Before the tasks were administered, subjects were informed not to consume any nicotine, caffeine or a large meal within 2-4 hours of the study. They were all requested to abstain from alcohol for at least 12 hours prior to the study.

All subjects were given task practice to resolve any misunderstanding of task instructions or performance difficulties. Then a series of 24 task blocks were presented, each lasting 90 sec, and allowance was made for breaks between each block. To minimize word repetition, while also providing for counterbalanced repetition of task materials for each task condition, we generated six different word sequences. Each of these sequences was presented four times, once for each set of task instructions and

each attended color. The order of the fixed and variable tasks and the attended color for each block was counterbalanced within and across subjects. For each block of the fixed target task, a different target word was selected at random, with no replacement.

This ERP experiment was conducted in conjunction with positron emission tomography (PET; Clark et al., 2000, 2003). There were two separate scanning sessions, so the order of the PET and ERP sessions were counterbalanced, with half of the subjects from each group doing the PET session first and other half doing the ERP session first.

3.2.3   EEG Acquisition

These methods follow common standards (e.g., Picton et al., 2000). EEG data were acquired continuously through a 128 channel *SYNAMPS* system with *ESI-128* software (NeuroScan, Sterling, VA, USA). EEG was recorded using medium and large *Electro-Caps* and *Electro-Gel* (Electro-Cap International [ECI], Eaton, OH, USA). *Electro-Caps* contained tin electrodes of 9 mm diameter (5 mm exposed, with a 2.5 mm hole, leaving a 2.5 mm doughnut shaped contact surface). Electrodes were positioned according to the extended 10-20 system of the American Electroencephalographic Society (1991; excluding Nz, F9, F10, and Cz from the 73 channels reported therein, with additional sites at: AFp3, AFp1, AFp2, AFp4, Fp1P, Fp2P, AF5, AF1, AF2, AF6, F7P, F5P, F3P, F1P, F2P, F4P, F6P, F8P, AT7, AC5, AC3, AC1, AC2, AC4, AC6, AT8, T7P, C5P, C3P, C1P, C2P, C4P, C6P, T8P, AP7, AP5, AP3, AP1, AP2, AP4, AP6, AP8, P3P, P1P, P2P, P4P, TPO7, TPO8, AO1, AO2, TO1, TO2, O1P, O2P, I1, I2; see also Oostenveld & Praamstra, 2001). All scalp EEG sites were grounded at AFz and referenced at A2; A1 was recorded with reference to A2 for off-line calculation of a linked ears reference (Picton, Lins & Scherg, 1995). Tin electrodes were used to record the vertical electro-oculogram (EOG) from above and below the right eye and the

horizontal EOG from the outer canthi of each eye. Electrode impedances were all less than 10 kΩ and within 5 kΩ of one another. EEG/EOG was amplified 1000/500 times, respectively, across a bandpass of DC-70 Hz and digitized at 2.5 ms intervals (at 16 bit resolution, 0.034 µV sensitivity & 2.2 mV range).

3.2.4 Cerebral Magnetic Resonance Imaging

Structural modeling of the cerebral tissues was based on magnetic resonance imaging (MRI). A high-resolution T1 weighted anatomical sequence was obtained with a magnetization prepared rapid acquisition gradient echo sequence (MPRAGE, Siemens Magnetom 4000 [Erlangen, Germany]; time to repetition = 12.5 ms, time to echo = 5 ms, flip angle = 10 degrees). The MRI volumes were corrected for RF inhomogeneity with the FSL FAST algorithm (Zhang, Brady & Smith, 2001). A shrink-wrapping method was used to obtain scalp models, which involved deformation of a spherical tessellation, guided by the intensity values of the MRI volume, so that vertices are located at the scalp boundary (EMSE; Source Signal Imaging).

3.2.5 Electrode Localization and MRI Coregistration

Electrode 3D positions were digitized using a *FASTRAK* device (Polhemus, Colchester, VT, USA) and the *3D-SPACE* software (NeuroScan, Sterling, VA, USA). The average inter-electrode distance was 1.97 ± 0.39 cm. During MRI acquisition, multi-modality radiographic markers (Neuromedical Supplies, Neurosoft) were placed on the left and right pre-auricular points and the nasion, which were then clearly identified in the MRI by intensity differentiation. These anatomical landmarks were also digitised during the EEG collection. Co-registration of the electrodes to the MRI head surface was first approximated by rigid alignment of the markers, with further adjustment given by a least squares fit algorithm (EMSE; Source Signal Imaging; see

Figure 3-2). The realistic coregistration of electrodes to the scalp surface was completed before computation of the Laplacian transform (discussed further below).
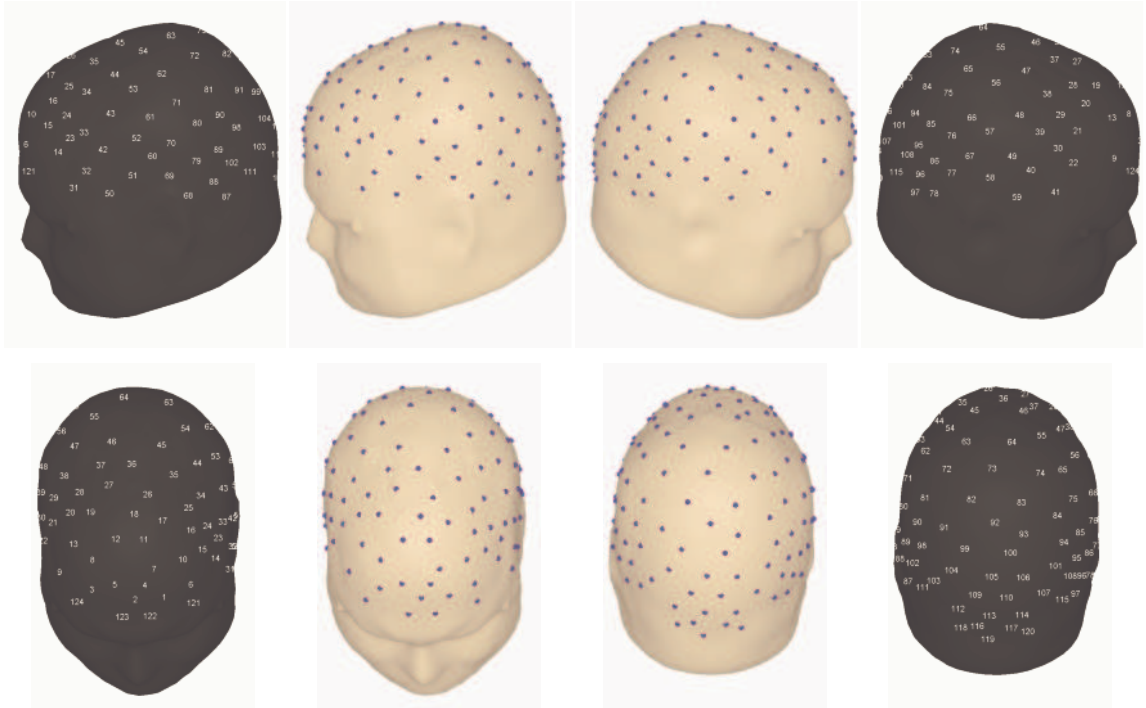

Figure 3-2. Realistic 3D electrode locations. Note that electrode locations are fairly evenly distributed. Also note that this montage has no Cz electrode.

3.2.6   EEG Preprocessing

Electromyographic (EMG) and direct current (DC) offset correction artifacts were manually removed; the EOG artifacts were mathematically corrected in all scalp channels (Semlitsch, Anderer, Schuster & Presslich, 1986). The EOG correction enabled the retention of trials that would be removed otherwise, which is particularly valuable when working with psychiatric populations who generate a lot of EOG artifacts. Data preprocessing involved careful evaluation of EOG correction parameters and visual inspection of the corrected data. Where any residual EOG artifact remained, it was often highly diminished and any trials that appeared to contain insufficient correction were manually rejected. EEG trials were epoched from 200 ms pre-stimulus to 1500 ms post-stimulus, baselined from -200 to 0 ms. Lastly, an automated rejection

pass excluded any trials if they contained any value greater than ±120 μV in any scalp electrode.

Averages were computed for each task condition, excluding all epochs with incorrect button-press responses. Some subject averages contained artifact data for some electrodes, indicated by maximal variance greater than 50 μV. There were no significant differences in the number of artifact electrodes between controls (12.5 ± 9.0) and patients (6.0 ± 5.4; t[18]=1.96, ns). Data from artifact electrodes were replaced with a linear weighted average of six good nearest neighbors (cf. spherical spline interpolations; e.g., Perrin, Pernier, Bertrand & Echallier, 1989). The nearest neighbors were determined from the 3D electrode coordinates, using the spherical arc length (given small distances, a sphere is a good approximation to the realistic surface).

3.2.7   Data Analysis

3.2.7.1   Behavioral Measures of Task Performance

The behavioral measures of task performance were target response time (RT), percentage of targets detected (%TD), and the percentage of false target detections (%FP, i.e. responses to non-targets). RT was recorded for each target response and averaged across all target presentations of each task. %TD was computed by dividing targets detected by 60 (total targets presented per task). %FP was computed as the number of responses to non-targets divided by 660 (total non-targets presented per task). These calculations were made after collapsing across the attended word color.

3.2.7.2   Analysis of Scalp Potential and Scalp Current Density

The EEG in this study was measured as a surface potential difference between active scalp sites and a non-cephalic reference, the right ear-lobe (A2). This reference channel was chosen to avoid distortion of the scalp topography that can arise from a

linked-ears reference (see Katznelson, 1981; Regan, 1989; Nunez, 1990). However, as we wished to compare the results here with previous findings from the linked-ears reference, the ERPs with a right-ear reference were mathematically transformed, off-line, to a linked-ears reference (see Regan, 1989; Picton et al., 1995). This provides, to some degree, continuity with the ERP literature; although the problems inherent in a linked-ears reference are best avoided, the literature largely reports results at mid-line sites (Fz, Cz & Pz), which are not as badly affected as lateralized topographic analysis. In any case, given the spatial smearing of scalp potentials by volume conduction through the high resistance of the skull, the ERPs are complemented by analyses of the scalp current density (SCD), which is a reference free estimation of focal scalp activity (Hjorth, 1975; Katznelson, 1981; Nunez, 1990; Perrin, Bertrand, Giard & Pernier, 1990). Furthermore, analyses of cortically constrained source estimation are in progress; although these results are not available here, similar results are given in Clark et al. (2001).

The SCD data was derived from a Laplacian transformation, based on digitization of 3D realistic electrode coordinates (*EMSE* software; Source Signal Imaging, San Diego, California, USA). The Laplacian was computed on the scalp potential recorded with a right-ear reference, using a spherical spline interpolation (based on Perrin, Bertrand & Pernier, 1987; Perrin, Bertrand, Pernier, Giard & Echallier, 1987; Perrin et al., 1989). The spherical spline was regularized by a lambda coefficient ($1x10^{-6}$) to avoid artifacts that can arise from noise in the ERP or aberrant electrode locations (see Wahba, 1990; Babiloni, Carducci, Babiloni & Urbano, 1998). Also, to approximate a realistic surface, the calculations defined the spherical radius independently for each electrode. Alternative methods, which were unavailable, include spline interpolation for an ellipsoid surface (Law, Nunez & Wijesinghe, 1993) or a realistic scalp surface (e.g., Le, Menon & Gevins, 1994; Babiloni et al., 1996, 1998; He, Lian & Li, 2001).

The SCD measure is a reference-free measure of scalp activity, which is becoming more common in the literature. It is reported here in units of current density (uA/m^3), which has the same polarity as the scalp voltage (these units are preferred in Pernier, Perrin & Bertrand, 1988; Perrin et al., 1990). To obtain this measure, the Laplacian of potential (uV/m^2) is multiplied by minus the scalp conductivity (S/m). The Laplacian values have also been reported previously in units of voltage (e.g., uV/m^2), which has an opposite polarity to the scalp potential, and these values are *proportional* to current density, where proportionality depends on conductivity (Katznelson, 1981). To facilitate comparison between the scalp ERP and the SCD, the current density units were preferred for this study.

To better understand the SCD measure, consider the electromagnetic properties of the EEG (see Jackson, 1999; Plonsey, 1969, 1982; Malmivuo & Plonsey, 1995; Nunez, 1995). The scalp EEG arises from superposition of volume conducted currents that are generated by synchronous activity in cortical pyramidal cells (see Nunez, 1981, 1990, 1995). The transmembrane currents of cortical pyramidal cell dendrites can be modeled as current dipoles that generate extracellular fields, where the macroscopic properties are summarized in Maxwell's equations. The cerebral tissues, comprising the brain, skull and scalp (among others), may be modeled as homogeneous, isotropic tissue compartments, characterized primarily by conductivity (σ). Given any distribution of source activity in the brain, the total cerebral current density (**J**) is given as the sum of both the source current density (**J**s) and the extracellular current density (**J**e),

$$\mathbf{J} = \mathbf{J}s + \mathbf{J}e$$

The extracellular current density can be considered as the product of the tissue conductivity (σ) and the strength of the electric field (**E**),

$$\mathbf{J}e = \sigma\mathbf{E}$$

So, by substitution, we have,

$$\mathbf{J} = \mathbf{J}s + \sigma\mathbf{E}$$

Also, the electric field can be considered in terms of electric potential (φ), which is often measured from biological tissues,

$$\mathbf{E} = -\nabla\varphi$$

Where del (∇, nabla) is the partial differential vector operator and $\nabla\varphi$ gives the gradient of the scalar potential field (φ). Again, by substitution, we have,

$$\mathbf{J} = \mathbf{J}s - \sigma\nabla\varphi$$

Note that there is zero divergence of the total current density ($\nabla \cdot \mathbf{J} = 0$), so

$$\nabla \cdot (\mathbf{J}s - \sigma\nabla\varphi) = 0$$

$$\nabla \cdot \mathbf{J}s - \nabla \cdot (\sigma\nabla\varphi) = 0$$

$$\nabla \cdot \mathbf{J}s = \nabla \cdot (\sigma\nabla\varphi)$$

Thus, the spatial distribution of potential is given by this partial differential equation (Poisson's equation; Nunez, 1995). "The source (or, more precisely, the current source density) $\mathbf{J}s(r,t)$ may result from very complex nonlinear neural interactions; however, once specified on a closed surface, the resulting potential is determined at locations external to the surface by the above linear equation." (Nunez, 1995, p. 21).

Source activity is located in the nervous system and we assume there are no active sources in the scalp, where we have,

$$\mathbf{J}s = 0$$

Hence, at the scalp,

$$-\nabla \cdot (\sigma\nabla\varphi) = 0$$

Also, if we assume that the scalp is a homogeneous, isotropic conductor, the conductivity (σ) is constant, so we have,

$$-\sigma (\nabla \cdot \nabla\varphi) = 0$$

$$-\sigma \nabla^2\varphi = 0$$

This relationship gives the product of the conductivity with the Laplacian of the potential (where ∇^2 is known as the Laplacian operator, which gives the second spatial derivative, also known as the divergence of the gradient). This quantity is the SCD, so we have the Laplacian of potential (V/m^2) multiplied by minus the scalp conductivity (Siemens/m). In this study, the scalp conductivity was estimated at 0.33 Siemens/m. The precise estimate of this value is problematic, but the value chosen is consistent with early physiological studies that have guided the development of recent modeling software (see Geddes & Baker, 1967; Rush & Driscoll, 1968, 1969; see also Nunez, 1987). Now we can see that the term 'scalp current density' (SCD) refers to a scalar field that represents the divergence of the current density vector field on the scalp surface (see also Katznelson, 1981).

We can further determine that this value is proportional to the normal component of the current density vector at a constant, infinitesimal depth below the scalp surface; it may be considered to indicate the degree of current flow into or out of the scalp (Pernier et al., 1988). This can be shown mathematically by considering the components of the Laplacian transform of potential,

$$\nabla^2\varphi = (\ \partial^2\varphi/\partial x^2,\ \partial^2\varphi/\partial y^2,\ \partial^2\varphi/\partial z^2\ )$$

In the scalp, we have,

$$\nabla^2\varphi = (\ \partial^2\varphi/\partial x^2,\ \partial^2\varphi/\partial y^2,\ \partial^2\varphi/\partial z^2\ ) = 0$$

so,

$$(\ \partial^2\varphi/\partial x^2,\ \partial^2\varphi/\partial y^2\ ) = -\ \partial^2\varphi/\partial z^2$$

or similarly in terms of the scalp surface normal ($\mathbf{n}$),

$$(\ \partial^2\varphi/\partial x^2,\ \partial^2\varphi/\partial y^2\ ) = -\ \partial^2\varphi/\partial n^2$$

Note that the z component is zero at the boundary of the scalp with air, because the air has zero conductivity, but it is not zero at the skull-scalp boundary or inside the scalp. Hence, the x and y components represent the surface Laplacian and the z component is

the current flow into the scalp from the brain (via the skull) in the radial or surface
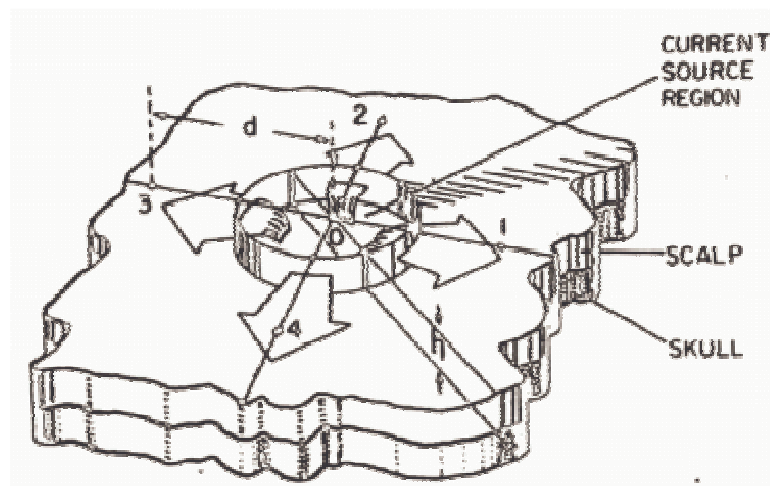
normal direction (see Figure 3-3).

Figure 3-3. A model of current flow from brain sources, through the skull, into the
scalp. The tissue compartments are assumed to be homogenous, isotropic conductors
(constant conductivity). Note that the current flowing into the scalp diverges into
tangential components (in x and y). The scalp surface Laplacian measures the
magnitude of this divergence (and convergence). Reprinted, with permission, from
Katznelson (1981).

The SCD enhances the spatial resolution of scalp potentials; "the Laplacian is a

spatial filter that emphasizes local sources and reduces the contribution of distant

sources" (Nunez, 1990, p. 30). Simulations indicate that the SCD is less sensitive to

distant or deep brain sources and more sensitive to near or shallow brain sources than

the scalp potential (Pernier et al., 1988; Oostendorp & van Oosterom, 1996). For

example, given a shallow and a deep source signal, the SCD resolves the shallow signal,

while the scalp potential indicates the deep signal (Pernier et al., 1988). The scalp

potential is a poor indication of high spatial frequency in the currents of shallow brain

generators. Nunez et al. (1994) used concentric sphere simulations to demonstrate that

scalp potentials are poorly correlated with cortical potential (r = 0.53) and only resolve

patches of coherent cortical activity of >5 cm diameter, regardless of electrode density

(e.g., 118 electrodes, 1 cm spacing; see also Srinivasan, Tucker & Murias, 1998). With

increasing density of scalp electrode arrays (48, 64, 118 electrodes), the Laplacian

estimate of SCD provides better estimates of cortical potential (r = .71, .78, & .94, respectively; Nunez et al., 1994; see also Nunez, Pilgreen, Westdorp, Law & Nelson, 1991). Thus, the SCD is a more reliable indication than scalp potential of shallow source contributions to scalp components.

3.2.7.3   Region Specific Component Identification and Analysis

In low-resolution ERP data analysis, it is common to measure the peak amplitude and latency of components at specific electrode sites. However, with high-resolution ERPs, it is clear that individual subjects demonstrate component peaks at similar scalp regions, but not identical electrode locations (e.g., Foxe & Simpson, 2002; see also Lehmann & Skrandies, 1984; Skrandies, 1989; Wang, Begleiter & Porjesz, 1994; Gevins et al., 1996; Neylan et al., 1999). Hence, a small spatial location adjustment is made for small variations in peak amplitude location across subjects, in order to better capture the peak activity for any scalp component. Given that the skull and scalp smear or blur the activity from brain source activity, with considerable anatomical variation across subjects, it may not be reasonable to rely on the structure of the 10-20 system. This system, unlike some structural normalization routines used in PET and fMRI analysis, does not take into account individual variations in anatomy, especially when it is used with electrode caps (despite some allowance for different cap sizes). Although this study does not attempt to apply structural normalization, using affine transformations and associated interpolation, to scalp recorded ERPs, we have adapted a simple smoothing procedure to the analysis of ERP activity. With high-density scalp arrays for ERP recording and analysis, we can adopt similar smoothing parameters to those used commonly in PET and fMRI analysis. In this study, the individual variation in peak location was accounted for by definition of discrete electrode groups (cf. Homan, Herman & Purdy, 1987; Lagerlund et al., 1993; Towle et al., 1993; see also

Gevins, Cutillo & Smith, 1995; Gevins et al., 1996). The scalp topography was

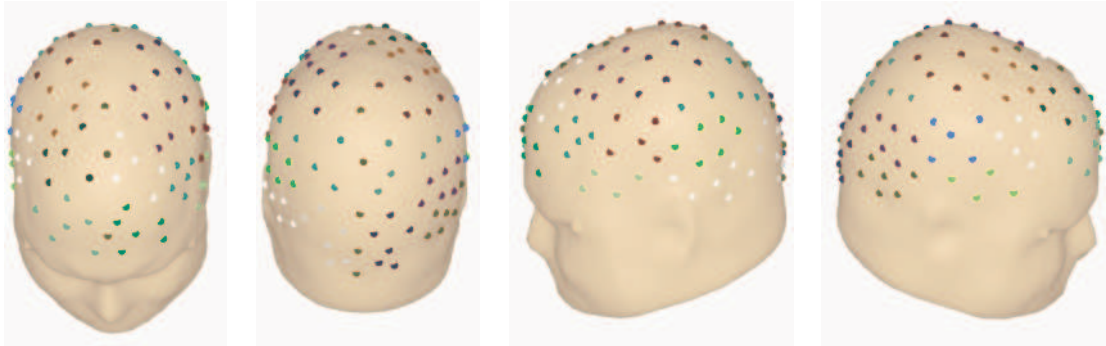segmented into 22 regions (see Table 3-1 & Figure 3-4).

Figure 3-4. An heuristic indication of the size of electrode regions on a realistic 3D
scalp. Each region has a random color allocation; in this case neighboring regions are
mostly different colors. Each region comprises a small group of 3-6 electrodes,
covering scalp areas of approximately 4-8 cm.

Table 3-1. Regional Electrode Allocations (labels from Oostenveld & Praamstra, 2001).

Region	Left Hemisphere	Right Hemisphere
Prefrontal		
Superior (SPF)	AFF5h, AFF1h, F3, F1, FFC1h	AFF2h, AFF6h, F2, F4, FFC2h
Inferior (IPF)	Fp1, AFp3, AF7, AF3, AFp9h, NFp1h	Fp2, AFp4, AF4, AF8, NFp2h, NFp2h
Frontal		
Superior (SF)	FFC3h, FC3, FC1, FCC3h, FCC1h	FFC4h, FC2, FC4, FCC2h, FCC4h
Inferior (IF)	F7, F5, FFT7h, FFC5h, FC5	F6, F8, FFC6h, FFT8h, FC6
Central		
Superior (SC)	C3, C1, CCP3h, CCP1h, CP1	C2, C4, CCP2h, CCP4h, CP2
Inferior (IC)	FTT7h, FCC5h, C5, TTP7h, CCP5h	FCC6h, FTT8h, C6, CCP6h, TTP8h
Parietal		
Superior (SP)	CP3, CPP3h, CPP1h, P1, PPO1h	CP4, CPP2h, CPP4h, P2, PPO2h
Inferior (IP)	CP5, TPP7h, CPP5h, P5, P3, PPO3h	CP6, CPP6h, TPP8h, P4, P6, PPO4h
Temporal		
Anterior (AT)	FT9, FT7, T9, T7	FT8, FT10, T8, T10
Posterior (PT)	TP9, TP7, P9, P7, PO9, POO9h	TP8, TP10, P8, P10, PO10, POO10h
Occipital (OC)	PO7, PO3, POO1, O1, OI1h, I1	PO4, PO8, POO2, O2, OI2h, I2

Note. Region labels in brackets are cited in the results chapters to follow.

ERP components were identified in the grand mean ERP waveforms and the ERP difference waveforms. The polarity and timing of components in the grand mean waveforms guided further automated analysis of individual subjects. Individual subject component measurements were made within a reasonable time-window of the grand mean latency, carefully defined so that peak detection routines avoid measurement of preceding or following peak components. All waveforms were low-pass filtered at 14 Hz before analysis to avoid spurious detection of outlying high frequency peaks and to facilitate accuracy of automated peak detection.

Given a time window for each component, automated routines measured the baseline to peak amplitude and latency of the maximum peak in a given electrode region for individual subjects (cf. Gevins et al., 1996). The electrode containing a peak for an experimental condition was used to find the corresponding peak for a control condition, to avoid confounding these within-subjects comparisons. Where no peak could be detected, the routine selected the maximal amplitude in a scalp region at the time of the grand mean peak. Values from the automated routine were verified by random manual inspection of individual subject's data.

3.2.7.4   *Inferential Statistics*

Independent samples t-tests and ANOVA or non-parametric equivalents were used to evaluate group differences in demographic attributes, clinical symptom ratings, and the number of EEG trials contributing to average ERPs for each condition. Two factor (task x group) repeated measures ANOVA was used to analyze response time and accuracy. Pearson's correlation coefficient was used to evaluate linear relationships between scalp electrical components, behavioral responses and clinical symptom ratings.

Unless hypotheses specified analysis of particular regions, the grand mean scalp topography for controls clearly indicated a regional focus of component activity, which was used to define specific regions for statistical analysis. From a full set of 11 bilateral regions, statistical analyses were restrained to one or two, with a mixed factorial ANOVA performed for a given bilateral region. Given the small group size and the importance of inferring significant group differences, it was important to avoid exploratory analyses and associated corrections for multiple comparisons. The region specific topographic analysis effectively simulates similar region of interest analyses employed generally in functional neuroimaging, which effectively reduces the impact of

type I errors. Furthermore, investigation with factor analyses of scalp topography from representative scalp components of this study often indicated no more than 2 topographic factors, accounting for at least 80% of the variance. This indicated that the effective topographic resolution of the component activity was about 2 spatial components (or resolution elements, RESELS), which is often used in neuroimaging studies to estimate the required correction for multiple comparisons. As these components are often bilateral, these comparisons were incorporated into region specific ANOVA analyses. The regions selected for analysis were based on clear focal activity in the group topography.

Region specific analyses of component amplitude and latency were analyzed with mixed-factor, within and between subjects ANOVA (SPSS GLM method). For any given component, the scalp topography indicated no more than two regions of maximal amplitude. To avoid complex interactions and reduce the number of analyses that may contribute to Type I errors, the regions of maximal amplitude were selected for specific region of interest analysis (cf., Gevins et al., 1996). Most often, these regions correspond well with expected locations of task related activity. The ERP data was assessed for normal distribution and equal variance across conditions and groups before application of a mixed factor ANOVA model to assess effects for group (2 between subject levels), condition (2 within subject levels for either attention, working memory or executive attention), and hemisphere (2 within subject levels for left and right). All mean differences are given after Bonferroni corrections for multiple comparisons. Where mean differences were predicted, it was possible to evaluate planned comparisons and 1-tailed p-values, which are reported as necessary.

3.2.8   Data Visualization

All graphics were generated within the author's Matlab™ toolbox (see,
http://eeg.sf.net/, accessed 01/2003). The realistic 3D topography of the grand mean
waveforms was visualized using the triangulated surface interpolation of Oostendorp,
Oosterom and Huiskamp (1989, method B). This method was developed, tested and
verified on simulated spherical surface data (available on request). It should be noted
that all grand mean waveforms and topographic maps are provided for heuristic
purposes, they are not intended to be a precise indication of the component
measurements and analyses, as the latter take into account intersubject variability in
both small regional location and latency. Also note that all waveform plots do not
include the EOG electrodes. Many studies report the EOG waveforms to indicate the
absence of EOG artifacts. These studies employ a method of single trial rejection for
any EOG artifact. In contrast, this study employed mathematical correction of EOG
artifacts during single trial data processing (Semlitsch et al., 1986), which leaves the
EOG waveforms intact, so they still contain large EOG deflections, while the impact of
those deflections on the EEG data has been removed.